

Nucleation and Growth of Silver Nanoparticles by AB and ABC-Type Atomic Layer Deposition

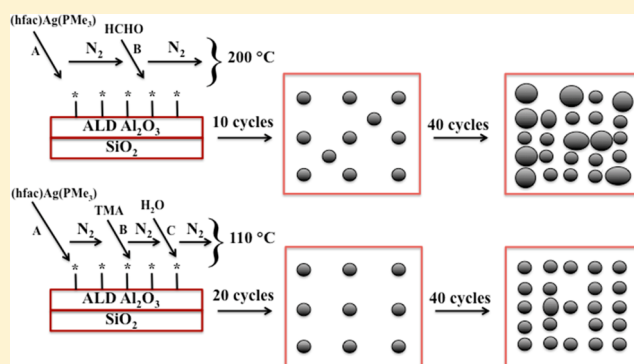
Sicelo S. Masango,[†] Lingxuan Peng,[‡] Laurence D. Marks,[‡] Richard P. Van Duyne,[†] and Peter C. Stair^{*,†,§,⊥}

[†]Department of Chemistry and the Institute for Catalysis in Energy Processes, Northwestern University, Evanston, Illinois 60208, United States

[‡]Department of Materials Science and Engineering, Northwestern University, Evanston, Illinois 60208, United States

Supporting Information

ABSTRACT: In this work, we report synthesis strategies to produce Ag nanoparticles by AB-type and ABC-type atomic layer deposition (ALD) using trimethylphosphine-(hexafluoroacetylacetonato) silver(I) ((hfac)Ag(PMe₃)) and formalin (AB-type) and (hfac)Ag(PMe₃), trimethylaluminum, and H₂O (ABC-type). In situ quartz crystal microbalance measurements reveal a Ag growth rate of 1–2 ng/cm²/cycle by ABC-type ALD at 110 °C and 2–10 ng/cm²/cycle for AB-type ALD at 170–200 °C. AB-type Ag ALD has a nucleation period before continuous linear growth that is shorter at 200 °C. Transmission electron microscopy reveals that AB-type Ag ALD particles have an average size of ~1.8 nm after 10 cycles. ABC-type Ag ALD particles have an average size of ~2.2 nm after 20 cycles. With increasing ALD cycles, ABC-type Ag ALD increases the metal loading while maintaining the particle size but AB-type Ag ALD results in the formation of bigger particles in addition to small particles. The ability to synthesize supported metal nanoparticles with well-defined particle sizes and narrow size distributions makes ALD an attractive synthesis method compared to conventional wet chemistry techniques.



INTRODUCTION

The ability to control the size, structure, and chemical composition of noble metal nanoparticles (NPs) is an ongoing endeavor in catalysis research. Noble metal NPs are of interest because of their unique chemical and optical properties. It is well-known that NPs can differ chemically from bulk materials owing to the reduced coordination numbers and high percentage of surface atoms¹ and should be tunable through better control of their size, shape, and structure.² Supported silver (Ag) NPs are an example of noble metal NPs that have been studied extensively. As a material, Ag is of interest due to its high electrical and thermal conductivity and its high optical reflectivity.³ Ag is also used in catalytic and plasmonics applications. In plasmonics, the localized surface plasmon resonance (LSPR) on Ag NPs leads to strongly enhanced local electric fields, which can be used to enhance Raman scattering in surface-enhanced Raman spectroscopy (SERS).^{4–7} The LSPR of Ag NPs can also be used to enhance fluorescence,⁸ luminescence,⁹ and photoabsorption.¹⁰

In catalysis, Ag NPs are used mainly as catalysts in the epoxidation of ethylene to form ethylene oxide (EO).¹¹ EO is used to make engine antifreeze, ethoxylates, plastics, and higher glycols.^{12–15} Recently, small alumina-supported Ag clusters (~3.5 nm) have been shown to be very active for direct propylene epoxidation to propylene oxide at low temperatures,

with negligible amounts of CO₂ formation.^{16,17} Conventional methods of preparing Ag catalysts include wet impregnation, coprecipitation, colloidal synthesis, ion-exchange, and chemical vapor deposition (CVD).^{2,18} These methods are reliable at producing catalytic materials but oftentimes NPs with a broad size distribution are formed. It remains a challenge to synthesize small Ag NPs with narrow size distributions on oxide supports.¹⁸

Atomic layer deposition (ALD) is a promising synthesis strategy that is under development for producing noble metal NPs on metal oxide supports. ALD is a thin film growth technique, which relies on self-limiting binary reactions between gaseous precursor molecules and a substrate to deposit uniform films in a layer-by-layer fashion.^{19–24} Many late transition metals tend to grow as islands of NPs on supports during the first few ALD cycles before growing into a film.²⁰ This so-called Volmer–Weber growth can be explained by the stronger interactions between the deposited metal atoms than with the support.^{2,25} Unlike wet chemical synthesis methods, ALD involves only the nanoparticle precursors, thereby minimizing possible contamination from solvents and

Received: April 25, 2014

Revised: July 3, 2014

surfactants and allows conformal deposition on most substrates regardless of whether they are flat, porous, or have challenging three-dimensional topologies.

Previously, supported Pt,^{26–28} Pd,^{29–32} Ir,³³ Ru,³⁴ Ru–Pt,³⁵ and Pt–Pd³⁶ NPs have been prepared by ALD. Only one study has reported the synthesis of Ag NPs by ALD.³⁷ To the best of our knowledge, there are no ALD studies that report the synthesis of Ag NPs on high surface area supports. The difficulty in performing Ag ALD has been attributed to the lack of stable and volatile Ag precursors.³ In this work, we report two ALD methods to produce supported Ag NPs. We present in situ quartz crystal microbalance (QCM) studies to explore how the Ag NPs nucleate and grow during ALD. We also study the morphology, size and size distribution of the particles using high-resolution transmission electron microscopy (HREM) and high-angle annular dark field (HAADF) imaging.

EXPERIMENTAL SECTION

Ag Atomic Layer Deposition. Ag ALD was performed in a home-built viscous flow reactor that is similar to others described previously.³⁸ Ultrahigh purity nitrogen (99.999%) flowed continuously through the reactor at 120 sccm. The operating pressure of the ALD system during Ag deposition was ~ 2 Torr. The Ag precursor was contained in a stainless steel bubbler which was heated to ~ 63 – 66 °C to achieve sufficient vapor pressure. Nitrogen at 154 sccm passed through the bubbler and assisted transport of the Ag precursor molecules to the reactor. To prevent precursor condensation, the reactor inlet lines were heated to ca. 100 °C by heating tapes controlled by individual variacs.

The Ag precursor used in this study was trimethylphosphine-(hexafluoroacetylacetonato) silver(I) ((hfac)Ag(PMe₃)) (Strem Chemicals, 99%). For AB-type ALD, (hfac)Ag(PMe₃) was the A precursor and formalin (formaldehyde, Sigma-Aldrich, 37 wt % in H₂O with 10% methanol in water added for stability) was the B precursor. The timing used for one AB-type ALD cycle is denoted as t_1 – t_2 – t_3 – t_4 seconds where t_1 is the dose time for A; t_2 is the purge time for A; t_3 is the dose time for B; and t_4 is the purge time for B. For ABC-type ALD, (hfac)Ag(PMe₃) was the A precursor, trimethylaluminum (TMA, Sigma-Aldrich, 97%) was the B precursor, and 18.2 MΩ cm⁻¹ Millipore H₂O was the C precursor. The timing for one ABC-type ALD cycle is denoted as t_1 – t_2 – t_3 – t_4 – t_5 – t_6 where t_1 is the dose time for A; t_2 is the purge time for A; t_3 is the dose time for B; t_4 is the purge time for B; t_5 is the dose time for C; and t_6 is the purge time for C. Formalin, TMA, and H₂O were contained in reservoirs maintained at room temperature.

Ag ALD on High Surface Area Supports. Ag ALD was also performed on high surface area silica gel (Silicycle S10040M, surface area ~ 100 m²/g, particle size of 75–200 μm, and an average pore diameter of 30 nm). Before ALD deposition, the silica gel was hydroxylated by immersing in boiling water for 2 h, followed by filtering and drying at 90 °C for 1 h.³⁹ The hydroxylated silica gel (~ 200 mg) was uniformly dispersed on a fixed-bed powder tray with a mesh top to contain the powder while still allowing access by the precursor vapors. The powder samples were loaded into the center of the reactor and dried overnight at the deposition temperature in a 120 sccm flow of nitrogen at ~ 1.5 Torr to achieve a consistent density of hydroxyl groups. The silica gel powder was modified using 20 ALD cycles of Al₂O₃ prior to Ag deposition. The Al₂O₃ acted as a seed layer for the Ag NPs and provided

hydroxyl groups.³⁰ The Al₂O₃ ALD used alternating exposures of TMA and H₂O using a timing of 60–180–240–240 s at 110 °C. Each cycle of Al₂O₃ deposits ca. 1.1 Å/cycle of oxide.¹⁹ AB-type Ag ALD was performed using a timing of 600–300–300–300 s. ABC-type Ag ALD was performed using the timing 600–300–90–240–120–240 s. Longer dose times are required to give precursors sufficient time to deposit on the silica gel and longer purge times help prevent precursor intermixing.⁴⁰

In Situ Quartz Crystal Microbalance (QCM) Studies. An in situ QCM (Inficon Q-POD +6 MHz Colorado Crystal Corp.) was used to monitor film growth. The QCM was fitted with a nitrogen purge on the backside to prevent backside deposition.

Transmission Electron Microscopy. The samples were characterized by conventional high-resolution transmission electron microscopy (HREM) and high-angle annular dark field (HAADF) imaging. A few milligrams of the samples were dispersed in 3 mL of ethanol then a few drops of this solution were deposited onto copper TEM grids with supported carbon film and dried in air. The average sizes and size distributions of the Ag NPs were determined from multiple HAADF images with a collection angle of 124–268 mrad. Both HREM and HAADF images were taken using a JEOL JEM-2100F operating at 200 kV.

RESULTS

In Situ QCM Studies. To meet ALD requirements, the precursors must be volatile, thermally stable, and exhibit self-limiting deposition. The ALD window, which is the temperature region of nearly ideal ALD behavior, must be known.¹⁹ (hfac)Ag(PMe₃) was chosen because it has been used to make thin films using CVD.⁴¹ Thermogravimetric analysis and QCM measurements (SI Figure S1) show that (hfac)Ag(PMe₃) is thermally stable and manifests self-limiting behavior.

AB-Type Ag ALD: QCM Studies. QCM measurements of AB-type Ag ALD were performed at different temperatures. Figure 1a shows linear growth at 170, 185, and 200 °C after a temperature dependent nucleation or incubation period. The nucleation period is shortest at 200 °C, with linear growth observed after as few as 10 cycles. An analogous nucleation period has been observed with Pd ALD at 200 °C.⁴² Figure 1b shows an expanded plot of the linear portion during growth at 200 °C, exhibiting a steady Ag growth rate of 10 ng/cm²/cycle.

ABC-Type Ag ALD: QCM Studies. The motivation for pursuing ABC-type Ag ALD follows from the successful deposition of Pd and Pt NPs by this method.^{18,30,43} The ABC method makes metal nanoparticle deposition possible at temperatures as low as 80 °C.¹⁸ Figure 2a shows QCM measurements for ABC-type Ag ALD at 110 °C. From a detailed examination of several cycles (Figure 2b), the average mass gain per cycle can be seen to be 2 ng/cm² (3.1×10^{12} molecules/cm²) from the (hfac)Ag(PMe₃) pulse and 25 ng/cm² from the combination of TMA and H₂O pulses. The Ag mass gain per ABC cycle is very low but can be increased by using multiple TMA/H₂O (BC) cycles in each ALD cycle as shown in SI Figure S2.

AB-Type Ag ALD: TEM Studies. Figure 3 shows a HAADF image of a sample synthesized by 10 AB-type Ag ALD cycles along with the particle size distribution. The resolution of the HAADF imaging is limited by the probe size. The size of the particles measured from the image is a convolution of the real particle size and the probe size. The data herein has been corrected for the size of the probe.

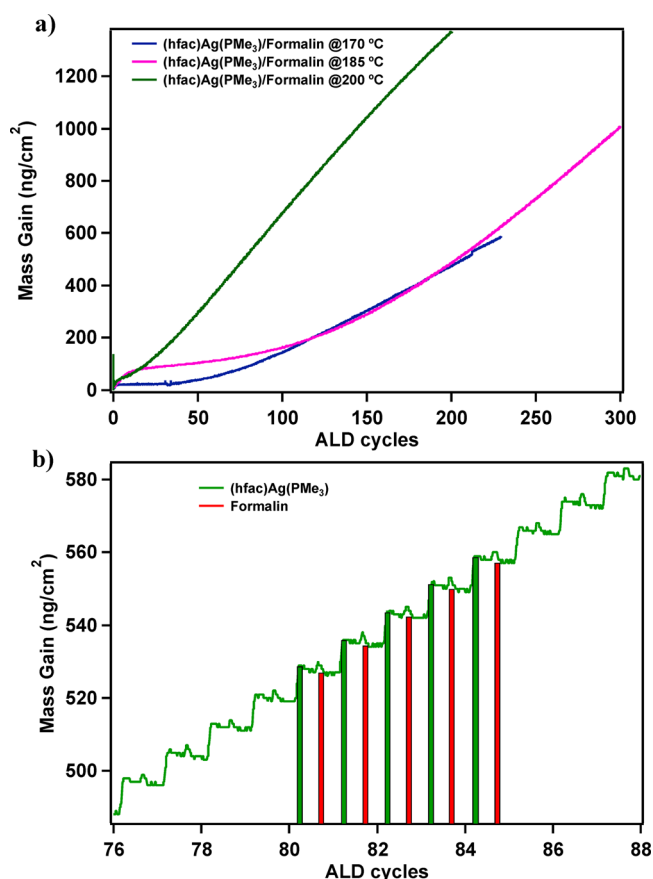


Figure 1. (a) Nucleation and growth of Ag on Al₂O₃ by AB-type ALD at 170 °C, 185 °C, and 200 °C measured by in situ QCM. (b) QCM measurements for AB-type Ag ALD growth at 200 °C and a timing sequence of 2–10–2–10 s.

The average size of the particles in Figure 3 (after removing a few bigger particles, fitting with a Gaussian and correcting for the probe effect) is 1.8 ± 0.4 nm. The Ag particles are approximately spherical in shape with ~ 180 Ag atoms each, assuming a density of 10.5 g/cm^3 . HREM images of the sample are provided in SI Figure S5. HAADF images for 20 and 40 AB-type Ag ALD cycles are included in SI Figure S6.

ABC-Type Ag ALD: TEM Studies. Figure 4 shows a HAADF image of a sample prepared by 20 ABC-type Ag ALD cycles and its size distribution. The average size of 267 Ag NPs is 2.2 ± 0.6 nm, containing ~ 330 Ag atoms each.

DISCUSSION

AB-Type Ag ALD: QCM Studies. Figure 1a reveals that AB-type Ag ALD works best at 200 °C since the nucleation period is significantly shortened. A possible reason for the very low initial Ag growth rate is the bulkiness of (hfac)Ag(PMe₃) and its ligands which block nucleation sites. For Pd ALD, X-ray photoelectron spectroscopy studies revealed that some of the hfac ligands remain bound to the surface, i.e., they are not completely removed by formalin.⁴² Despite the interference from hfac ligands on the surface, the reported Pd growth rate (0.2 \AA/cycle) is higher than that of Ag (calculated to be 0.07 \AA/cycle at 200 °C). It is possible that the hfac ligands are bound more strongly to Ag than Pd, which makes them harder to remove by formalin. We did not investigate ALD temperatures above 200 °C to avoid precursor decomposition.

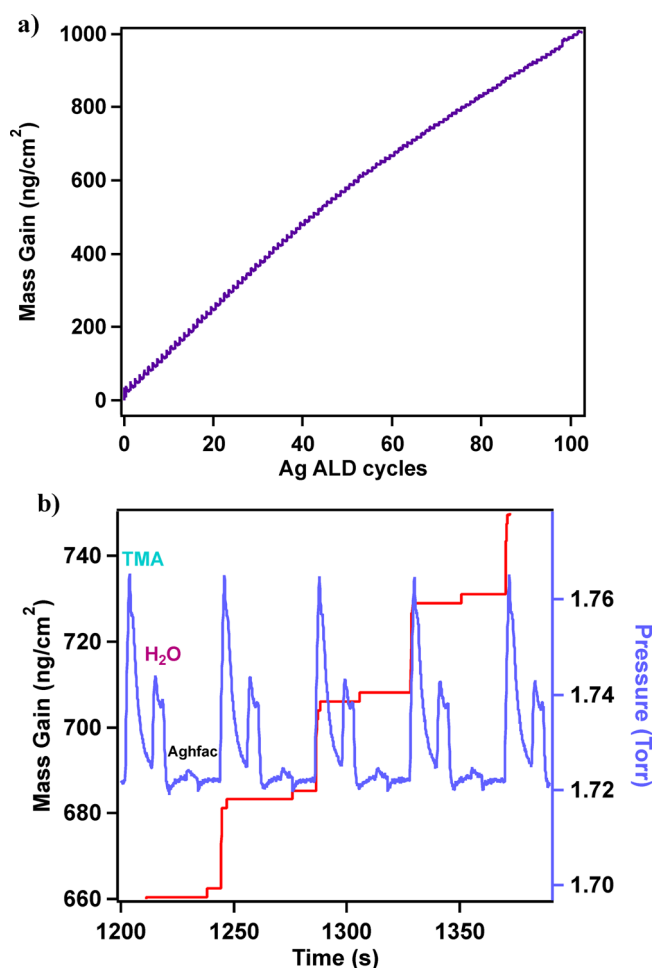
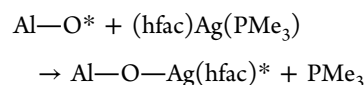


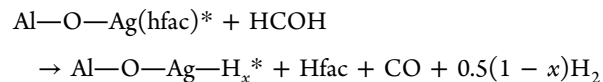
Figure 2. (a) In situ QCM measurements of mass gain during ABC-type Ag ALD on Al₂O₃ at 110 °C. For each cycle, the mass gain from the (hfac)Ag(PMe₃) pulse is 2 and 25 ng/cm² from the combination of TMA and H₂O pulses. (b) Expanded view of ABC-type Ag ALD showing mass gains (red) and pressures (blue) during (hfac)Ag(PMe₃), TMA, and H₂O exposures.

A likely sequence of reactions that describes the growth of Ag NPs on Al₂O₃ surfaces is given below. The reaction of (hfac)Ag(PMe₃) on Al₂O₃ is as follows:

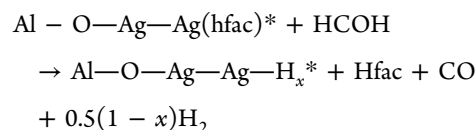
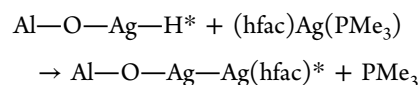


where the asterisks designate surface species.

Upon exposure to formalin, the reaction is as follows:



In the linear growth regime, the reactions are as follows:



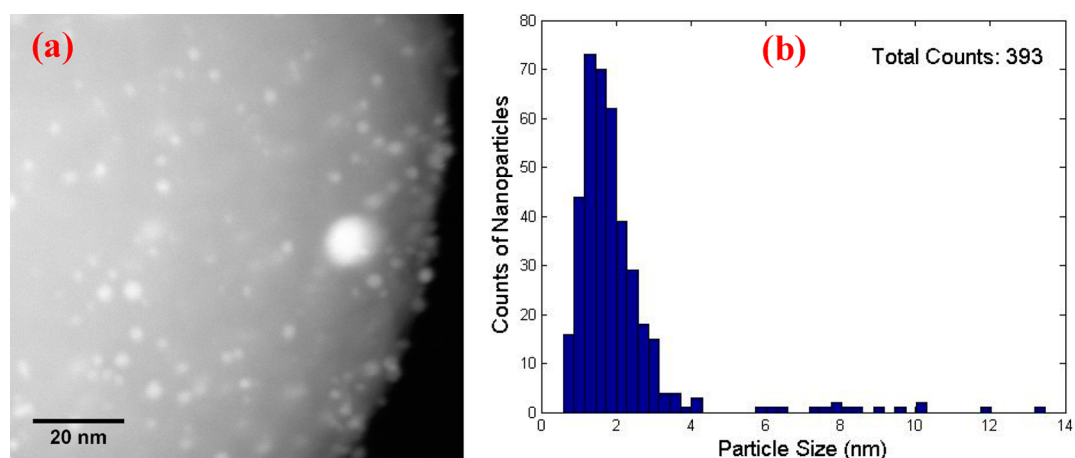


Figure 3. HAADF image (a) and the size distribution histogram (b) of as-prepared 10 AB-type Ag ALD NPs on alumina-coated silica gel at 200 °C.

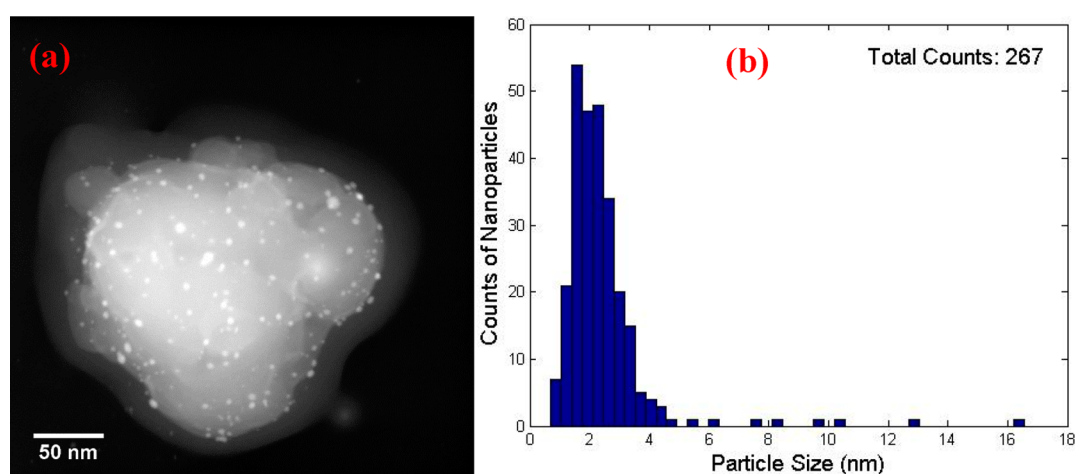


Figure 4. HAADF image (a) of as-prepared Ag NPs by 20 cycles ABC-type ALD on alumina-coated silica gel at 110 °C and the size distribution histogram (b).

A similar set of reactions has been proposed for Pd ALD using $\text{Pd}(\text{hfac})_2$ and formalin as precursors.^{42,45}

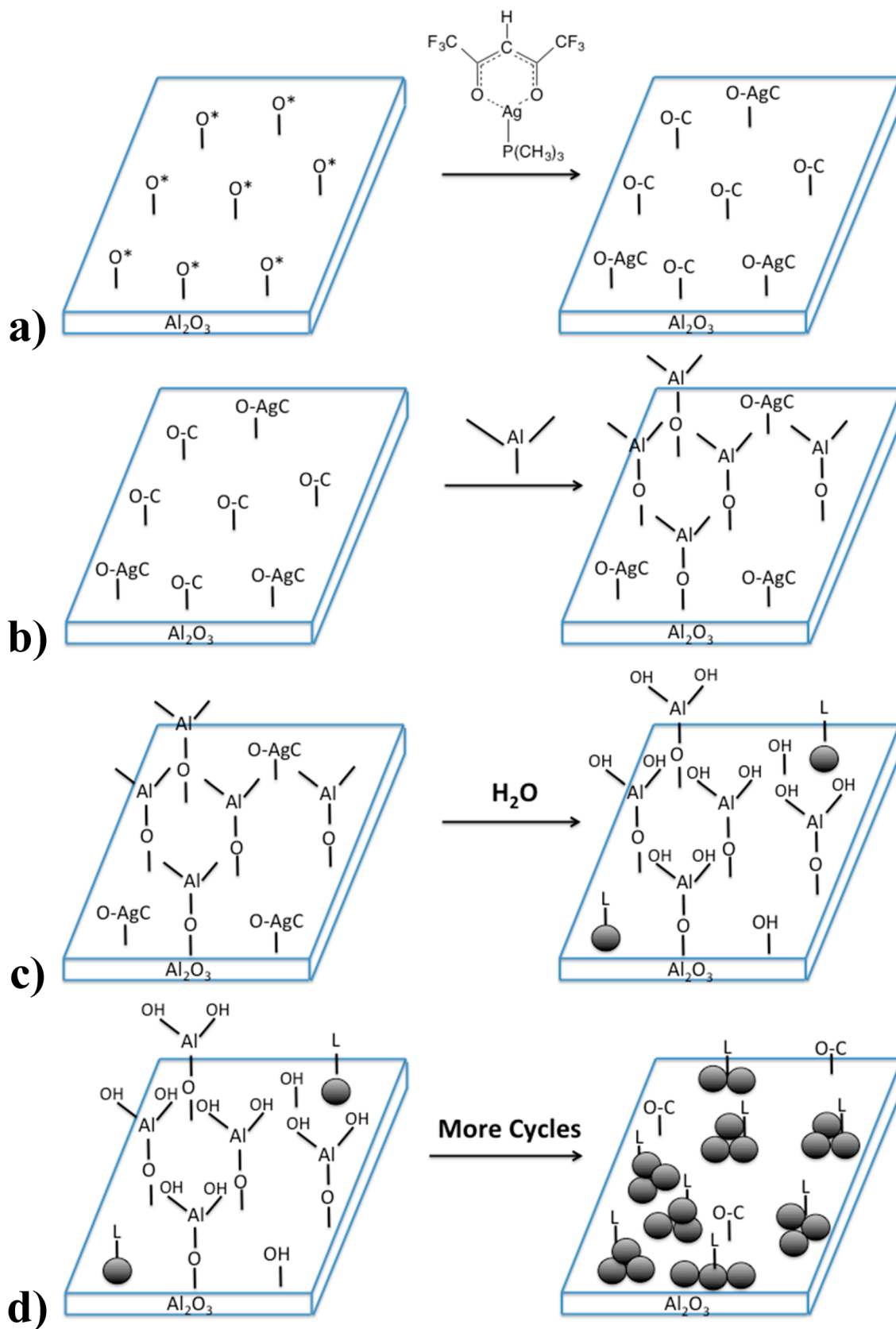
ABC-Type Ag ALD: QCM Studies. The QCM measurements (Figure 2) show that ABC-type Ag ALD is possible at temperatures as low as 110 °C. At this temperature, AB-type Ag ALD is impractical as a consequence of a very long nucleation period caused by the slow removal of adsorbed hfac ligands. Higher temperatures of ~200 °C are usually required to remove the hfac species at a reasonable rate.^{30,42} The mass gains from $(\text{hfac})\text{Ag}(\text{PMe}_3)$ during ABC-type ALD can be increased by dosing multiple BC (TMA/ H_2O) cycles as shown in SI Figure S2. We believe that multiple TMA/ H_2O cycles create more nucleation sites for $(\text{hfac})\text{Ag}(\text{PMe}_3)$.

The observation that multiple TMA/ H_2O cycles are needed to maximize Ag growth can be explained by surface “poisoning” with hfac ligands. It has been shown by Goldstein et al. that the adsorption of $\text{Pd}(\text{hfac})_2$ on Al_2O_3 yields $\text{Pd}(\text{hfac})^*$ and $\text{Al}(\text{hfac})^*$. Through in situ Fourier transform infrared spectroscopy studies, they showed that $\text{Al}(\text{hfac})^*$ species cause surface poisoning and TMA removes these species.⁴⁴ By analogy with this work, we propose that dosing $(\text{hfac})\text{Ag}(\text{PMe}_3)$ on Al_2O_3 results in $\text{Ag}(\text{hfac})^*$ and $\text{Al}(\text{hfac})^*$ surface species and that the $\text{Al}(\text{hfac})^*$ species prevent additional nucleation of $(\text{hfac})\text{Ag}(\text{PMe}_3)$. This is supported by SI Figure S3 which shows that Al_2O_3 has a low growth rate on a surface

saturated with a layer of $(\text{hfac})\text{Ag}(\text{PMe}_3)$. Removal of the poisoning species requires several TMA exposures before a typical Al_2O_3 linear growth rate is observed.

Scheme 1 depicts the deposition of Ag by ABC-type ALD. (a) $(\text{hfac})\text{Ag}(\text{PMe}_3)$ adsorbs on nucleation sites (believed to be $\text{Al}-\text{OH}/\text{Al}-\text{O}$ sites) and dissociates into $\text{Ag}(\text{hfac})^*$ and $\text{Al}(\text{hfac})^*$ species indicated by AgC and C, respectively. (b) TMA reacts with $\text{Al}(\text{hfac})^*$ and generates $\text{Al}(\text{CH}_3)^*$ surface species as previously shown by Goldstein et al.⁴⁴ (c) H_2O regenerates OH groups which act as nucleation sites during subsequent $(\text{hfac})\text{Ag}(\text{PMe}_3)$ exposures. The removal of $\text{Al}(\text{hfac})^*$ species by TMA frees up space on the surface allowing some of the $\text{Ag}(\text{hfac})^*$ species to diffuse and form Ag nanoclusters. The L on the Ag nanoclusters represents remaining hfac ligands on the Ag NPs. (d) With more ALD cycles, more nucleation sites are generated and this facilitates the growth of Ag NPs on the surface.

AB-Type and ABC-Type Ag ALD: Particle Size and Loading. The average size of AB-type Ag ALD NPs is 1.8 ± 0.4 nm after 10 cycles as shown in Figure 3. For 20 cycles of ABC-type ALD, the Ag NPs are 2.2 ± 0.6 nm (Figure 4). Both methods have a narrow size distribution. For AB-type Ag ALD, TEM studies show that some of the particles increase in size when the number of cycles is increased to 40. SI Figure S6g shows that the bigger particles have an average size of ~19 nm

Scheme 1. Proposed Schematic Showing ABC-Type Ag ALD Nucleation and Growth on Al_2O_3 ^a

^a(a) $(\text{hfac})\text{Ag}(\text{PMe}_3)$ adsorbs on nucleation sites (depicted by O^*) and dissociates into $\text{Ag}(\text{hfac})^*$ and $\text{Al}(\text{hfac})^*$ species indicated by AgC and C , respectively. (b) TMA reacts with $\text{Al}(\text{hfac})^*$ species and generates $\text{Al}(\text{CH}_3)^*$ surface species (nucleation sites). $\text{Ag}(\text{hfac})^*$ species diffuse on the surface and form Ag nanoclusters. (d) With more cycles, Ag NPs nucleate and grow on the surface.

for 40 AB-type cycles. We also observe very small Ag NPs with an average size of ~ 1 nm after 40 AB-type cycles as shown in SI Figure S6d. In comparison, for 40 ABC-type ALD cycles, the average particle size remains almost constant ($\sim 2\text{--}3$ nm), independent of the number of cycles as shown in SI Figure S7c,d.

In general, for AB-type Pd ALD, it was observed that the NP size increases with the number of ALD cycles.³⁰ Ag NPs follow a similar behavior. Since AB-type Ag ALD is performed at 200 °C, small Ag NPs diffuse on the surface and agglomerate to form bigger NPs. This opens up nucleation sites from which small Ag NPs nucleate and grow hence the observation of very small Ag NPs in addition to bigger NPs even after 40 cycles of AB-type ALD.

For ABC-type Ag ALD, the NP size is nearly constant while the Ag loading increases as shown in SI Figures S7 and S8. This makes ABC-type ALD an ideal synthesis method to increase Ag loading without changing particle size, similar to ABC-type Pd ALD.³⁰ For the same number of ALD cycles, the Ag loading on the powder substrate is higher for AB-type ALD than ABC-type ALD (SI Figure S8). This is consistent with QCM studies which show more Ag mass deposited for AB-type ALD at 200 °C than ABC-type ALD at 110 °C (SI Figure S4). Overall, the loading of the Ag NPs is lower for both methods (SI Figure S8) in comparison to conventional synthesis methods.^{46–48}

The small, uniform Ag NP size may be advantageous as a component of active and selective catalysts. The avoidance of solvents, stabilizers, and polymers, which often require removal by high temperature calcination, may also be beneficial.

CONCLUSIONS

We have demonstrated that ALD can be used to synthesize supported Ag nanoparticles on silica gel powder. The Ag nanoparticles were synthesized by ABC-type and AB-type ALD methods at 110 and 200 °C respectively. In situ QCM measurements indicate that AB-type Ag ALD has a nucleation period before linear growth and the nucleation period is much shorter at 200 °C. Multiple TMA and H₂O cycles during ABC-type ALD can create nucleation sites on the surface and enhance adsorption of (hfac)Ag(PMe₃). The supported Ag nanoparticles have an average size of ~ 2 nm and a narrow size distribution for both methods.

TEM studies show that ABC-type Ag nanoparticles do not change size significantly even after 40 cycles, and this demonstrates the viability of ABC-type ALD to increase metal loading without changing nanoparticle size. In contrast, very small (~ 1 nm) nanoparticles are still observed even after 40 cycles of AB-type ALD in addition to bigger (~ 19 nm) nanoparticles. Low temperature ABC-type Ag ALD is highly desirable since it increases the metal loading while keeping the nanoparticle size nearly constant.

ASSOCIATED CONTENT

Supporting Information

HREM, HAADF images, and size distribution histograms of Ag nanoparticles prepared by AB-type and ABC-type ALD, TGA, and in situ QCM studies. This material is available free of charge via the Internet at <http://pubs.acs.org>.

AUTHOR INFORMATION

Corresponding Author

*E-mail: pstair@northwestern.edu.

Present Addresses

[§]Chemical Sciences and Engineering Division, Argonne National Laboratory, 9700 South Cass Avenue, Argonne, IL 60439.

[†]Department of Chemistry and the Center for Catalysis and Surface Science, Northwestern University, Evanston, IL 60208.

Notes

The authors declare no competing financial interest.

ACKNOWLEDGMENTS

The authors gratefully acknowledge financial support from the Northwestern University Institute for Catalysis in Energy Processes (ICEP). ICEP is funded through the US Department of Energy, Office of Basic Energy Science (Award Number DE-FG02-03-ER15457).

REFERENCES

- (1) Narayanan, R.; El-Sayed, M. A. Catalysis with Transition Metal Nanoparticles in Colloidal Solution: Nanoparticle Shape Dependence and Stability. *J. Phys. Chem. B* **2005**, *109*, 12663–12676.
- (2) Weber, M. J.; Mackus, A. J. M.; Verheijen, M. A.; Marel, C.; Kessels, W. M. M. Supported Core/Shell Bimetallic Nanoparticles Synthesis by Atomic Layer Deposition. *Chem. Mater.* **2012**, *24*, 2973–2977.
- (3) Niskanen, A.; Hatanpaa, T.; Arstilla, K.; Leskela, M.; Ritala, M. Radical-Enhanced Atomic Layer Deposition of Silver Thin Films Using Phosphine-Adducted Silver Carboxylates. *Chem. Vap. Deposition* **2007**, *13*, 408–413.
- (4) Willets, K. A.; Van Duyne, R. P. Localized Surface Plasmon Resonance Spectroscopy and Sensing. *Annu. Rev. Phys. Chem.* **2007**, *58*, 267–297.
- (5) Schatz, G. C.; Van Duyne, R. P. Electromagnetic Mechanism of Surface-Enhanced Spectroscopy. In *Handbook of Vibrational Spectroscopy*; Chalmers, J. M., Griffiths, P. R., Eds.; Wiley: New York, 2002; pp 759–774.
- (6) Whitney, A. V.; Elam, J. W.; Zou, S.; Zinovev, A. V.; Stair, P. C.; Schatz, G. C.; Van Duyne, R. P. Localized Surface Plasmon Resonance Nanosensor: A High-Resolution Distance-Dependence Study Using Atomic Layer Deposition. *J. Phys. Chem. B* **2005**, *109*, 20522–20528.
- (7) Jeanmaire, D. L.; Van Duyne, R. P. Surface Raman Spectroelectrochemistry. Part I. Heterocyclic, Aromatic, and Aliphatic Amines Adsorbed on the Anodized Silver Electrode. *J. Electroanal. Chem. Interfacial Electrochem.* **1977**, *84* (1), 1–20.
- (8) Weitz, D. A.; Garoff, S.; Gersten, J. I.; Nitzan, A. The Enhancement of Raman Scattering, Resonance Raman Scattering, and Fluorescence From Molecules Adsorbed on a Rough Silver Surface. *J. Chem. Phys.* **1983**, *78*, 5324–5338.
- (9) Achermann, M. Exciton-Plasmon Interactions in Metal-Semiconductor Nanostructures. *J. Phys. Chem. Lett.* **2010**, *1*, 2837–2843.
- (10) Standridge, S. D.; Schatz, G. C.; Hupp, J. T. Distance Dependence of Plasmon-Enhanced Photocurrent in Dye-Sensitized Solar Cells. *J. Am. Chem. Soc.* **2009**, *131*, 8407–8409.
- (11) Christopher, P.; Linic, S. Shape- and Size-Specific Chemistry of Ag Nanostructures in Catalytic Ethylene Epoxidation. *ChemCatChem* **2010**, *2*, 78–83.
- (12) Ozbek, M. O.; van Santen, R. A. The Mechanism of Ethylene Epoxidation Catalysis. *Catal. Lett.* **2013**, *143*, 131–141.
- (13) Campbell, C. T. The Selective Epoxidation of Ethylene Catalyzed by Ag (111): A Comparison with Ag (110). *J. Catal.* **1985**, *94*, 436–444.
- (14) van Santen, R. A.; de Groot, C. P. M. The Mechanism of Ethylene Epoxidation. *J. Catal.* **1986**, *98*, 530–539.
- (15) Lambert, R. M.; Williams, F. J.; Cropley, R. L.; Palermo, A. Heterogeneous Alkene Epoxidation: Past, Present and Future. *J. Mol. Catal. A: Chem.* **2005**, *228*, 27–33.
- (16) Lei, Y.; Mehmood, F.; Lee, S.; Greeley, J.; Lee, B.; Seifert, S.; Winans, R. E.; Elam, J. W.; Meyer, R. J.; Redfern, P. C.; et al. Increased

Silver Activity for Direct Propylene Epoxidation via Subnanometer Size Effects. *Science* **2010**, *328*, 224–228.

(17) Cheng, L.; Yin, C.; Mehmood, F.; Liu, B.; Greeley, J.; Lee, S.; Lee, B.; Seifert, S.; Winans, R. E.; Teschner, D.; et al. Reaction Mechanism for Direct Propylene Epoxidation by Alumina-Supported Silver Aggregates: The Role of the Particle/Support Interface. *ACS Catal.* **2014**, *4*, 32–39.

(18) Lu, J.; Stair, P. C. Low-Temperature ABC-type Atomic Layer Deposition: Synthesis of Highly Uniform Ultrafine Supported Metal Nanoparticles. *Angew. Chem., Int. Ed.* **2010**, *49*, 2547–2551.

(19) George, S. M. Atomic Layer Deposition: An Overview. *Chem. Rev.* **2010**, *110*, 111–131.

(20) Stair, P. C. Advanced Synthesis for Advancing Heterogeneous Catalysis. *J. Chem. Phys.* **2008**, *128*, 182507.

(21) Ritala, M.; Leskela, M. Atomic Layer Deposition. In *Handbook of Thin Film Materials*; Nalwa, H. S., Ed.; Academic Press: San Diego, CA, 2002; pp 103–159.

(22) Puurunen, R. L. Surface Chemistry of Atomic Layer Deposition: A Case Study for the Trimethylaluminum/Water Process. *J. Appl. Phys.* **2005**, *97*, 121301.

(23) Suntola, T. Atomic Layer Epitaxy. *Thin Solid Films* **1992**, *216*, 84–89.

(24) Miikkulainen, V.; Leskelä, M.; Ritala, M.; Puurunen, R. L. Crystallinity of Inorganic Films Grown by Atomic Layer Deposition: Overview and General Trends. *J. Appl. Phys.* **2013**, *113*, 021301.

(25) Campbell, C. T. Ultrathin Metal Films and Particles on Oxide Surfaces: Structural, Electronic and Chemisorptive Properties. *Surf. Sci. Rep.* **1997**, *27*, 1–111.

(26) Christensen, S. T.; Elam, J. W.; Rabuffetti, F. A.; Ma, Q.; Weigand, S. J.; Lee, B.; Seifert, S.; Stair, P. C.; Poepelmeier, K. R.; Hersam, M. C.; et al. Controlled Growth of Platinum Nanoparticles on Strontium Titanate Nanocubes by Atomic Layer Deposition. *Small* **2009**, *5*, 750–757.

(27) Baker, L.; Cavanagh, A. S.; Seghete, D.; George, S. M.; Mackus, A. J. M.; Kessels, W. M. M.; Liu, Z. Y.; Wagner, F. T. Nucleation and Growth of Pt Atomic Layer Deposition on Al₂O₃ Substrates Using (Methylcyclopentadienyl)-Trimethyl Platinum and O₂ Plasma. *J. Appl. Phys.* **2011**, *109*.

(28) Li, J.; Liang, X.; King, D. M.; Jiang, Y.-B.; Weimer, A. W. Highly Dispersed Pt Nanoparticle Catalyst Prepared by Atomic Layer Deposition. *Appl. Catal., B* **2010**, *97*, 220–226.

(29) Feng, H.; Libera, J. A.; Stair, P. C.; Miller, J. T.; Elam, J. W. Subnanometer Palladium Particles Synthesized by Atomic Layer Deposition. *ACS Catal.* **2011**, *1*, 665–673.

(30) Lu, J.; Stair, P. C. Nano/Subnanometer Pd Nanoparticles on Oxide Supports Synthesized by AB-type and Low-Temperature ABC-type Atomic Layer Deposition: Growth and Morphology. *Langmuir* **2010**, *26*, 16486–16495.

(31) Lu, J.; Elam, J. W.; Stair, P. C. Synthesis and Stabilization of Supported Metal Catalysts by Atomic Layer Deposition. *Acc. Chem. Res.* **2013**, *46*, 1806–1815.

(32) Lu, J.; Fu, B.; Kung, M. C.; Xiao, G.; Elam, J. W.; Kung, H. H.; Stair, P. C. Coking- and Sintering-Resistant Palladium Catalysts Achieved Through Atomic Layer Deposition. *Science* **2012**, *335*, 1205–1208.

(33) Vuori, H.; Silvennoinen, R. J.; Lindblad, M.; Osterholm, H.; Krause, A. O. I. Beta Zeolite-Supported Iridium Catalysts by Gas Phase Deposition. *Catal. Lett.* **2009**, *131*, 7–15.

(34) Biener, J.; Baumann, T. F.; Wang, Y.; Nelson, E. J.; Kucheyev, S. O.; Hamza, A. V.; Kemell, M.; Ritala, M.; Leskela, M. Ruthenium/Aerogel Nanocomposites via Atomic Layer Deposition. *Nanotechnology* **2007**, *18*, 055303.

(35) Christensen, S. T.; Feng, H.; Libera, J. A.; Guo, N.; Miller, J. T.; Stair, P. C.; Elam, J. W. Supported Ru-Pt Bimetallic Nanoparticle Catalysts Prepared by Atomic Layer Deposition. *Nano Lett.* **2010**, *10*, 3047–3051.

(36) Lei, Y.; Liu, B.; Lu, J.; Lobo-Lapidus, R. J.; Wu, T.; Feng, H.; Xia, X.; Mane, A. U.; Libera, J. A.; Greeley, J.; et al. Synthesis of Pt-Pd Core-Shell Nanostructures by Atomic Layer Deposition: Application

in Propane Oxidative Dehydrogenation to Propylene. *Chem. Mater.* **2012**, *24*, 3525–3533.

(37) Chalker, P. R.; Romani, S.; Marshall, P. A.; Rosseinsky, M. J.; Rushworth, S.; Williams, P. A. Liquid Injection Atomic Layer Deposition of Silver Nanoparticles. *Nanotechnology* **2010**, *21*, 405602.

(38) Elam, J. W.; Groner, M. D.; George, S. M. Viscous Flow Reactor with Quartz Crystal Microbalance for Thin Film Growth by Atomic Layer Deposition. *Rev. Sci. Instrum.* **2002**, *73*, 2981.

(39) Hermes, S.; Zacher, D.; Baunemann, A.; Woll, C.; Fischer, R. A. Selective Growth and MOCVD Loading of Small Single Crystals of MOF-5 at Alumina and Silica Surfaces Modified with Organic Self-Assembled Monolayers. *Chem. Mater.* **2007**, *19*, 2168–2173.

(40) Libera, J. A.; Elam, J. W.; Pellin, M. J. Conformal ZnO Coatings On High Surface Area Silica Gel Using Atomic Layer Deposition. *Thin Solid Films* **2008**, *516*, 6158–6166.

(41) Yuan, Z.; Dryden, N. H.; Vittal, J. J.; Puddephatt, R. J. Chemical Vapor Deposition of Silver. *Chem. Mater.* **1995**, *7*, 1696–1702.

(42) Elam, J. W.; Zinovev, A.; Han, C. Y.; Wang, H. H.; Welp, U.; Hryn, J. N.; Pellin, M. J. Atomic Layer Deposition of Palladium Films on Al₂O₃ Surfaces. *Thin Solid Films* **2006**, *515* (4), 1664–1673.

(43) Stair, P. C. Synthesis of Supported Catalysts by Atomic Layer Deposition. *Top. Catal.* **2012**, *55*, 93–98.

(44) Goldstein, D. N.; George, S. M. Surface Poisoning in the Nucleation and Growth of Palladium Atomic Layer Deposition with Pd(hfac)₂ and Formalin. *Thin Solid Films* **2011**, *519*, 5339–5347.

(45) Feng, H.; Elam, J. W.; Libera, J. A.; Setthapun, W.; Stair, P. C. Palladium Catalysts Synthesized by Atomic Layer Deposition for Methanol Decomposition. *Chem. Mater.* **2010**, *22*, 3133–3142.

(46) Boutros, M.; Trichard, J.-M.; Da Costa, P. Silver Supported Mesoporous SBA-15 as Potential Catalysts for SCR NO_x by Ethanol. *Appl. Catal., B* **2009**, *91*, 640–648.

(47) Zhu, W.; Han, Y.; An, L. Silver Nanoparticles Synthesized From Mesoporous Ag/SBA-15 Composites. *Microporous Mesoporous Mater.* **2005**, *80*, 221–226.

(48) Liu, H.; Ma, D.; Blackley, R. A.; Zhou, W.; Bao, X. Highly Active Mesostructured Silica Hosted Silver Catalysts for CO Oxidation Using the One-Pot Synthesis Approach. *Chem. Commun.* **2008**, 2677–2679.